JOURNAL OF CATALYSIS **170,** 390–401 (1997)
ARTICLE NO. CA971776

NO Adsorption, Desorption, and Reduction by CH_4 over Mn-ZSM-5

Adam W. Aylor, Lisa J. Lobree, Jeffrey A. Reimer, and Alexis T. Bell

Center for Advanced Materials, Lawrence Berkeley National Laboratory, and Department of Chemical Engineering, University of California, Berkeley, California 94720

Received March 14, 1997; revised June 5, 1997; accepted June 6, 1997

An investigation of the interaction of NO with Mn-ZSM-5 as well as the reduction of NO by methane has been conducted using *in situ* infrared spectroscopy and mass spectrometry. Adsorption of NO at room temperature on Mn^{2+} results in the slow oxidation to Mn^{3+}, with the simultaneous formation of N_2O. During NO exposure the intensity of the band for Mn^{2+}(NO) (1894 cm^{-1}) decreases while that for $Mn^{3+}(O^-)$(NO) (1966 cm^{-1}) increases. Elevating the temperature, or introducing O_2, converts the $Mn^{3+}(O^-)$(NO) to NO_2/NO_3 species. Adsorbed NO_2/NO_3 species are more stable to high temperature than NO. During the reduction of NO by CH_4 in the presence of O_2, NO_2 is formed via the oxidation of NO. Adsorbed NO_2 then reacts with CH_4. Cyanide species are observed and found to react very rapidly with NO_2, leading to the formation of N_2 and CO_2. A series of elementary steps are proposed to account for the reduction of NO by CH_4 in the presence of O_2. As a part of this mechanism, it is hypothesized that the formation of N_2 and N_2O occurs via the processes $Mn^{3+}(O^-)(CN) + NO_2 \rightarrow Mn^{3+}(O^-) + CO_2 + N_2$, and $Mn^{3+}(O^-)(CN) + NO_2 \rightarrow Mn^{2+} + CO_2 + N_2O$, respectively.

INTRODUCTION

There has been considerable interest recently in the use of metal-exchanged zeolites for the selective reduction (SCR) of NO by methane (1–22). Co-, Mn-, and Ni-exchanged ZSM-5, mordenite, and ferrierite catalysts have particularly high activity (1, 10, 14). Attempts to explain the mechanism by which CH_4 reduces NO over these catalysts have been restricted to Co-exchanged zeolites. Several studies have shown that the rate of NO reduction is considerably more rapid when O_2 is added to the feed (1, 2, 10, 13, 14, 18) and that in such circumstances NO_2 is formed rapidly by the reaction of NO with O_2. It has been proposed that CH_4 activation involves the reaction of CH_4 with adsorbed NO_2 (20, 21), and isotopic labeling experiments suggest that CH_4 activation is the rate limiting step (17). More recently, both cyanide and isocyanate species have been identified by *in situ* infrared spectroscopy on Co-ZSM-5 (21). Transient-response experiments suggest that cyanide species are likely intermediates and that their reaction with NO_2 leads to N_2 and CO_2 (22).

The present work is devoted to an investigation of the interactions of NO with Mn-ZSM-5 and the reduction of NO by CH_4. Infrared (IR) spectroscopy, together with temperature-programmed desorption (TPD) and reaction spectroscopy, is used to elucidate the nature of adsorbed species and the elementary processes involved in NO adsorption, desorption, and reduction by CH_4. Similarities between the behavior of Mn-ZSM-5 and Co-ZSM-5 are noted.

EXPERIMENTAL

Na-ZSM-5 was obtained from UOP. About 15 g of the zeolite was added to a 3.5-liter solution of 0.01 *M* manganese acetate. This mixture was stirred at 298 K for 23 h, then at 313 K for 20 h, and finally at 353 K for 24 h (1). The zeolite was filtered, washed, and dried overnight in a vacuum oven at 393 K. Elemental analysis of the catalyst determined the Si/Al ratio to be 16.2, and the Mn/Al ratio to be 0.36.

For infrared spectroscopy, 20–50 mg of the manganese-exchanged zeolite was pressed into a self-supporting wafer and placed into a flow-through infrared cell (volume = 0.126 cm^3) similar to that described by Joly *et al.* (23). Spectra were recorded on a Digilab FTS-50 Fourier-transform infrared spectrometer at a resolution of 4 cm^{-1}. Typically, 64 or 256 scans were coadded to obtain a good signal-to-noise ratio. A reference spectrum of Mn-ZSM-5 in He, taken at the same temperature as the experimental spectrum, was subtracted from each spectrum. The catalyst temperature was raised at the rate of 1.0 K/min when infrared spectra were recorded under conditions of temperature-programmed desorption or reaction. The total gas flow rate was 100 cm^3/min unless otherwise noted.

Conventional TPD and TPR experiments were carried out with 0.1 g catalyst sieved to 35–60 mesh and placed in a quartz microreactor. For these experiments, 2000 ppm NO was adsorbed on the catalyst at room temperature. The catalyst was purged with He for 15 min to remove weakly adsorbed NO, and then a temperature ramp of 8.0 K/min was initiated. NO was desorbed into either He or 0.5% O_2/He flowing at 100 cm^3/min, and the desorbing species were monitored by a mass spectrometer (UTI 100 C).

0021-9517/97 $25.00

For the present studies, 4.99% NO in He, 1.03% NO_2 in He, 2.14% CH_4 in He, and 10.1% O_2 in He were obtained from Matheson, and ^{15}NO and $^{13}CH_4$ were obtained from Isotec. UHP helium was obtained on-site. The He, NO, and CH_4 cylinders were passed through an oxysorb trap, an ascarite trap, and a molecular sieve trap, in that order, for additional purification. The O_2 was passed through an ascarite and a molecular sieve trap.

With the exception of the cases stated, prior to each experiment the catalyst was: (i) heated at 773 K for 30 min in a He stream containing approximately 5000 ppm NO and 9% O_2, (ii) heated at 773 K for 20 min in 10% O_2, (iii) heated at 773 K in He for about 3 h, and (iv) cooled to the desired temperature in helium.

To determine its activity, the catalyst was placed in a quartz microreactor. Reactants were supplied through mass flow controllers and the product composition was determined by gas chromatography. A molecular sieve 5A column was used to separate NO, O_2, N_2, CO, and CH_4. A Porapak Q column was also employed to separate CO_2 and N_2O. Typical reaction mixtures contained 5000 ppm NO, 5000 ppm CH_4, and 2.0% O_2, with the balance He. A 0.20-g sample of the catalyst was used with a total flow rate of 100 cm^3/min, resulting in a GHSV = 15,000 (based on an apparent bulk density of the zeolite of 0.5 g/cm^3). Prior to each activity measurement the catalyst was: (i) heated to 773 K in O_2 for 1 h, (ii) heated at 773 K in He for 1.5 h, and (iii) cooled to the desired reaction temperature in He. The conversion of NO was based on the amount of N_2 or N_2O formed and the conversion of CH_4 was based on the amount of CO_2 formed. CO was not observed under any conditions.

RESULTS

Adsorption and Desorption of NO

Figure 1A shows a series of spectra taken at room temperature during exposure to 5400 ppm NO. Sharp bands are observed at 2132 and 1894 cm^{-1}. Weak bands are also seen at 2275, 2250, 2240, 1966, and 1630 cm^{-1}. The intensity of the band at 1894 cm^{-1} decreases with time, whereas the features at 1630, 1966, and 2132 cm^{-1} increase. The bands at 2240–2275 cm^{-1} remain essentially unchanged. The band at 1894 cm^{-1} is in the range usually assigned to nitrosyls, and we therefore assign it to $Mn^{2+}(NO)(OH^-)$ (21, 24, 25). It is assumed that in order to charge compensate a single Al, the manganese is introduced as $Mn^{2+}(OH^-)$. For clarity, the OH^- group associated with $Mn^{2+}(OH^-)$ will not be indicated in future assignments. The band at 1966 cm^{-1} is at the high end of the range of values for nitrosyl adsorption and is in fact quite close to the value for $Co^{2+}(NO)$ (21). The presence of this band appears to be associated with the oxidation of Mn^{2+} to Mn^{3+} (*vide infra*), and, therefore, we tentatively assign this feature to $Mn^{3+}(O^-)(NO)$. The bands at 2275, 2250, and 2240 cm^{-1} are due to adsorbed N_2O, as confirmed by direct N_2O adsorption. The feature at 2132 cm^{-1} is present not only on Mn-ZSM-5 but also on H-ZSM-5, Na-ZSM-5, and Co-ZSM-5 and has been observed by several authors on Cu-ZSM-5 (24, 26–28). A careful investigation of this feature on Cu-ZSM-5 suggests that it is attributable to $NO_2^{\delta+}$ associated with Brønsted acid sites (28). The intensity of the band at 2132 cm^{-1} can be increased or decreased by either oxidizing or reducing Mn-ZSM-5, respectively. The band at 1630 cm^{-1} is in the region typical of NO_2/NO_3 species (25), but is also characteristic of H_2O. Adsorption of ^{15}NO at room temperature does not cause a shift in the

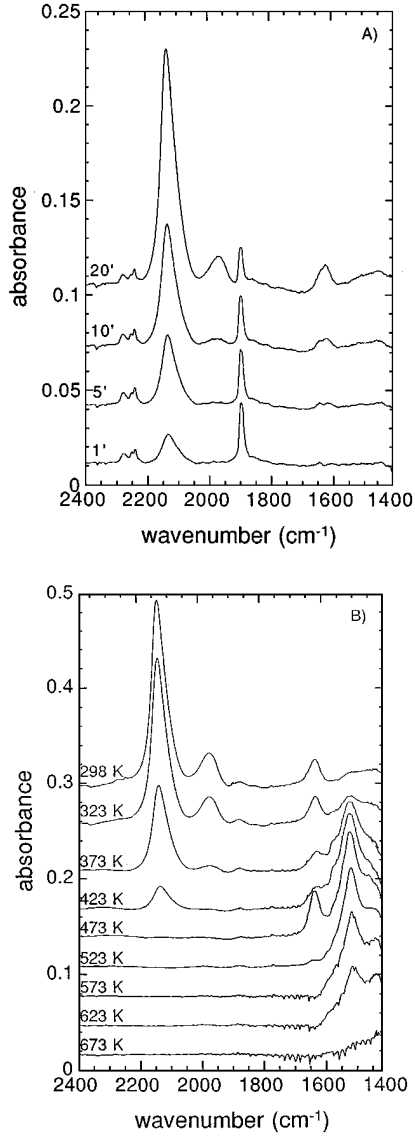

FIG. 1. Infrared spectra taken as a function of time during room-temperature exposure (A) and during temperature-programmed desorption after 20 min exposure (B) of the catalyst (standard pretreatment) to 5400 ppm NO in He.

position of this band, indicating that it is most likely due to adsorbed H_2O (25). The concurrent increase in the intensities of the bands at 1630 and 2132 cm^{-1} suggests that both H_2O and $NO_2^{\delta+}$ are formed simultaneously.

Figure 1B shows a series of infrared spectra taken during temperature-programmed heating of the catalyst after it had been exposed to 5400 ppm of NO for 20 min at room temperature. Purging in He at room temperature causes almost complete removal of the bands at 2275, 2250, 2240, and 1894 cm^{-1}. The band at 1966 cm^{-1} decreases in intensity below 423 K, whereas the band at 2132 cm^{-1} is observable below 473 K. The feature at 1516 cm^{-1}, along with shoulders at 1567 and 1591 cm^{-1}, grows to a maximum intensity at 473 K and then declines, and disappears completely above 623 K. Figure 1B also shows that at 473 K a rather intense band appears at 1630 cm^{-1}, which can be assigned to nitrato species (25). The position of the band at 1516 cm^{-1} is very similar to that for nitrito species in Co-A and Co-Y (29, 30) and in Co-ZSM-5 (20, 21) and is, therefore, assigned to $Mn^{3+}(O^-)(ONO)$. The features at 1561 and 1567 cm^{-1} are best assigned to monodentate and bidentate nitrato species, respectively (25).

A series of spectra taken during room temperature adsorption of 5800 ppm NO on a catalyst that had been heated at 773 K for 3 h in 10% O_2, cooled to room temperature in 10% O_2, and purged in He at room temperature for 30 min are shown in Fig. 2. The band at 1894 cm^{-1} again decreases in intensity with duration of exposure to NO. A band now grows in at 1935 cm^{-1}, and the NO_2/NO_3 species become evident at room temperature. The band at 1935 cm^{-1} is more easily attenuated when the infrared cell is purged with He

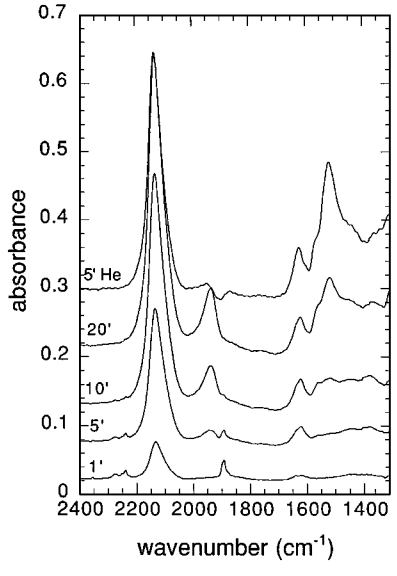

FIG. 2. Infrared spectra taken as a function of time during room-temperature exposure of the catalyst (oxidative pretreatment) to 5400 ppm NO in He.

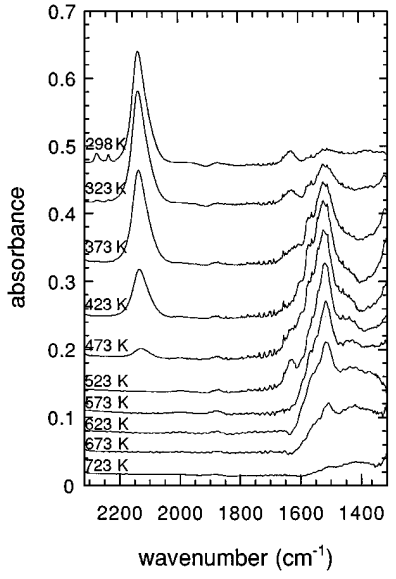

FIG. 3. Infrared spectra taken during temperature-programmed desorption into a He stream containing 1.8% O_2 following room-temperature exposure of the catalyst (standard pretreatment) to 5300 ppm NO for 20 min.

than the band at 1966 cm^{-1}. The position of the band at 1935 cm^{-1} suggests that it also can be assigned to a nitrosyl associated with Mn^{3+} cations. Since it grows with time in conjunction with the nitrito band, we tentatively assign the band at 1935 cm^{-1} to $Mn^{3+}(O^-)(ONO)(NO)$. The shift in frequency from 1966 to 1935 cm^{-1} is consistent with the addition of the electron donating ONO group. The band at 2132 cm^{-1} is approximately four times as intense after pretreatment of the catalyst in O_2. Desorption of the adsorbed surface species in He follows a pattern similar to that observed in Fig. 1B. Because the intensity of the nitrito band is large, this band continues to be observable up to 723–100 K higher than what is observed when the catalyst is given a standard pretreatment.

Figure 3 shows spectra for NO desorption into 1.8% O_2 after NO adsorption at room temperature for 20 min from a stream containing 5300 ppm NO on a catalyst given the standard pretreatment. The nitrito band reaches an intensity that is intermediate between that observed during TPD into He for a catalyst that has been given a standard and oxidative pretreatment. Presumably some of the NO that desorbs from the species giving rise to the band at 2132 cm^{-1} is oxidized to NO_2 and readsorbed on manganese cations.

TPD spectra for NO and its decomposition products are shown in Fig. 4. Prior to this experiment the catalyst is exposed to 2000 ppm of NO in He for 15 min at room temperature. The total amounts of NO, N_2O, O_2, and NO_2 are given in the figure legend. N_2O desorbs in a single peak at 410 K. By contrast, NO desorbs over the entire temperature range, with peaks evident at 355, 510, and 685 K. O_2

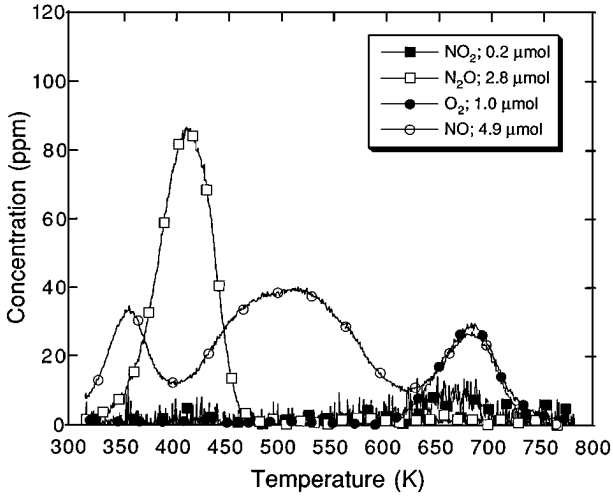

FIG. 4. Mass spectrometer signals for NO, N_2O, NO_2, and O_2 observed during the temperature-programmed desorption following room-temperature exposure of the catalyst (standard pretreatment) to 2000 ppm NO for 15 min.

desorbs in one high-temperature peak coinciding with the desorption of NO at 685 K. There is also a small amount of NO_2 which desorbs at 665 K.

NO TPD into He was performed after varying exposure times. The TPD spectra are shown in Fig. 5. NO desorption profiles are shown in Fig. 5A. The amount of NO desorbing from the first peak decreases with increasing adsorption time, while the second and third desorption peaks increase in intensity with increasing adsorption time. Figure 5B shows both N_2O and O_2 spectra on the same axis. N_2O desorption only occurs at temperatures below 500 K, and O_2 only desorbs above 600 K. N_2O desorption increases with adsorption time, and the peak maximum shifts from 450 to 410 K. O_2 desorption also increases with increasing adsorption time, and the peak is coincident with the high-temperature NO desorption peak. A detectable level of NO_2 is observed only after 900 s of NO adsorption.

Figure 6 shows TPD spectra for NO desorption into 0.5% O_2/He. The features for NO occurring between 310 and 450 K when the carrier gas is He are now gone, and two desorption peaks are evident at 525 and 670 K. Compared to desorption into He (see Fig. 4), the total amount of NO desorbing decreases by approximately 10%. N_2O desorption is reduced by 20%, and the peak position is shifted to lower temperature by 10 K. By contrast, the amount of NO_2 desorbed increases from about 0.2 to 1.3 μmol.

The processes envisioned to occur during the adsorption and desorption of NO on Mn-ZSM-5 are summarized in Fig. 7. At room temperature, most of the Mn is taken to be present as Mn^{2+} [viz., $Mn^{2+}(OH^-)$]. NO adsorption via reaction 1 produces $Mn^{2+}(NO)$ ($\nu = 1894$ cm^{-1}). This species reacts with additional NO to form $Mn^{3+}(O^-)$ and N_2O via reaction 2. The presence of N_2O is detected in the gas phase at room temperature when NO is passed over the catalyst and the effluent gas analyzed by mass spectrometry, as well as by the detection of bands at 2275, 2250, and 2240 cm^{-1} for adsorbed N_2O (Figs. 1A and 2). $Mn^{3+}(O^-)$ can adsorb NO to form $Mn^{3+}(O^-)(NO)$ ($\nu = 1966$ cm^{-1}) (reaction 3). Preoxidation of the catalyst leads to the formation of $Mn^{3+}(O_2^-)$. While the presence of $Mn^{3+}(O_2^-)$ is not observed directly, the observation of CO_2 during CO TPR of a preoxidized catalyst indicates that Mn undergoes oxidation. $Mn^{3+}(O_2^-)$ is presumed to react with NO at room temperature via reaction 5 to form $Mn^{3+}(O^-)(ONO)$ ($\nu = 1516$ cm^{-1}). Finally, adsorption of an additional molecule of NO via reaction 6 forms $Mn^{3+}O^-(NO)(ONO)$ ($\nu = 1935$ cm^{-1}) (Fig. 2).

The interpretation of TPD of adsorbed NO is best done by considering separately the processes occurring in the temperature ranges of 298–600 K and 600–773 K. (Note: Due to experimental considerations, the TPD-IR and TPD-MS experiments were run at different heating rates, i.e., 1 K/min versus 8 K/min. As a consequence, peaks associated with a given elementary process will occur at a lower temperature in the TPD-IR experiments than in the TPD-MS experiments.) Between 298 and 600 K, Figs. 4 and 5 show that NO and N_2O are the only species released into the gas phase. The infrared spectra in Fig. 1B show the disappearance of the bands for $Mn^{2+}(NO)$, $Mn^{3+}(O^-)(NO)$, N_2O, and $H^+(NO_2^{\delta+})$, and the concurrent growth in intensity of the bands for nitrite and nitrate species over this temperature range. The infrared and TPD observations can be reconciled in the following manner. As the temperature is raised above 298 K, NO begins to desorb from $Mn^{2+}(NO)$ (the reverse of reaction 1), contributing to the lowest temperature NO peak seen in the TPD spectra presented in Figs. 4 and 5. The decrease in intensity of this TPD peak with increasing exposure to NO at room temperature (see Fig. 5) is attributed to the progressive conversion of $Mn^{2+}(NO)$ to more strongly bound $Mn^{3+}(O^-)(NO)$ via reactions 2 and 3. In the range 350–600 K, several processes occur simultaneously: the decomposition of $H^+(NO_2^{\delta+})$ and $Mn^{3+}(O^-)(NO)$ (the reverse of reaction 3) to release NO, the conversion of $Mn^{3+}(O^-)(NO)$ to Mn^{2+} and NO_2 (reaction 7), the rapid disproportionation of NO to form N_2O and $Mn^{3+}(O^-)$ (reactions 1 and 2), and the adsorption of NO_2 to form nitrite and nitrate species (reactions 8 and 9). The consumption of NO_2 in this temperature range is so rapid that none emerges in the effluent gas. It is also observed that the disproportionation of NO is so rapid between 373 K and 473 K that it contributes to a corresponding decrease in the release of NO into the gas phase.

Above 600 K, Figs. 4 and 5 show desorption of NO and O_2. NO_2 is also observed for the longest exposure time. The infrared spectra presented in Fig. 1B show that the only adsorbed species contributing to the appearance of gas phase products are nitrite and nitrate species. The appearance of

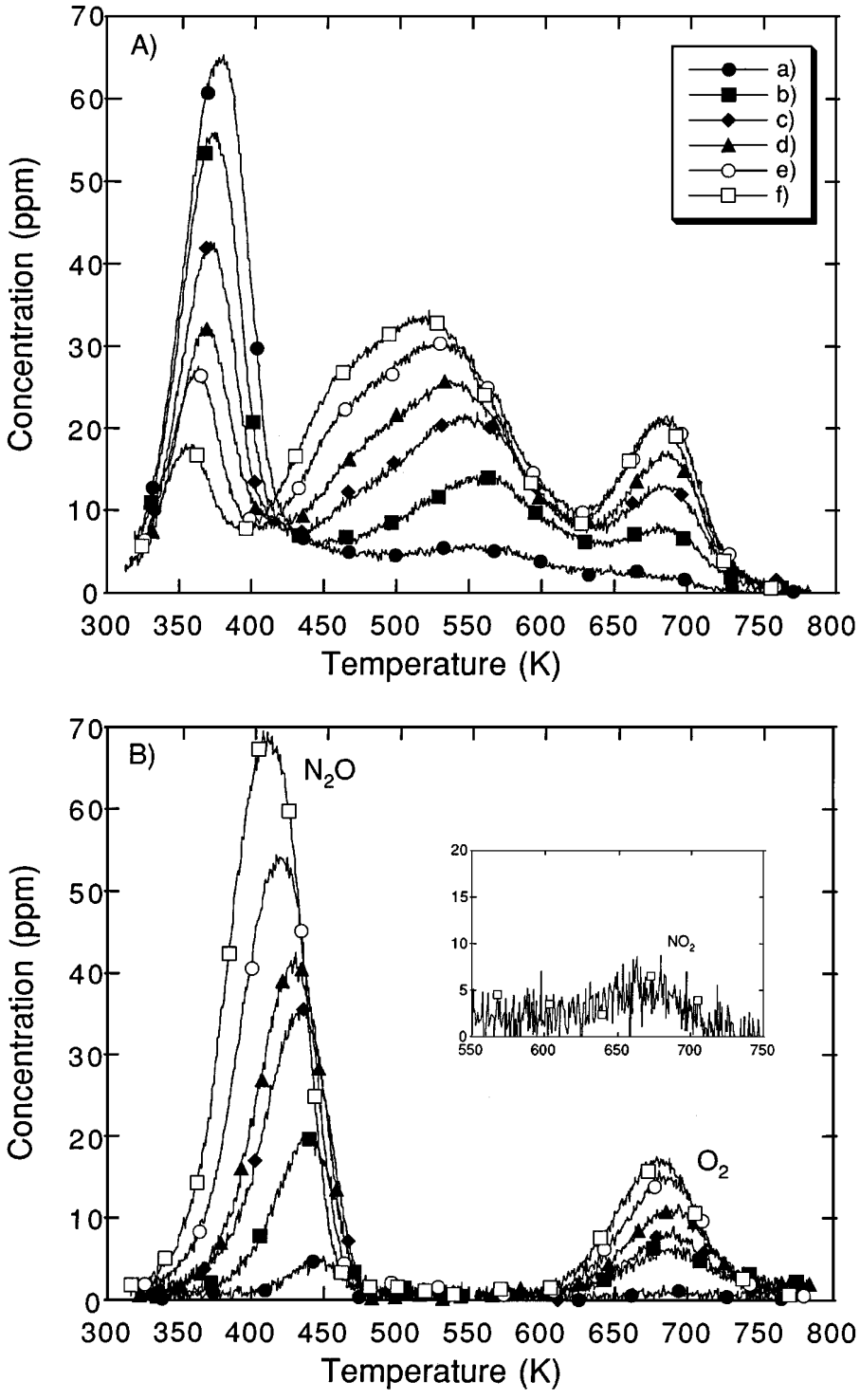

FIG. 5. Mass spectrometer signals for NO (A) and N_2O, O_2, and NO_2 (B), observed during the temperature-programmed desorption following room-temperature exposure of the catalyst (standard pretreatment) to 2000 ppm NO for 50 s (a), 75 s (b), 100 s (c), 200 s (d), 400 s (e), and 900 s (f).

NO and O_2 in a 1 : 1 ratio over the range 600–773 K is very likely due to decomposition of $Mn^{3+}(O^-)(ONO)$ to produce NO and O_2 (reaction 10). Comparison of curves (e) and (f) in Fig. 5 shows that in conjunction with desorption of NO_2, O_2 desoprtion increases, but NO desorption does not. The formation of NO_2, and this additional oxygen, is believed to represent the decomposition of nitrate species via reaction 11.

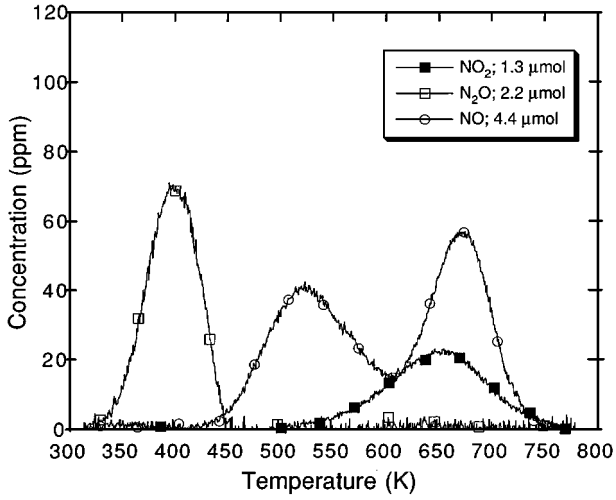

FIG. 6. Mass spectrometer signals for NO, N_2O, and NO_2 observed during the temperature-programmed desorption into a stream containing 5000 ppm O_2 in He, following room-temperature exposure of the catalyst (standard pretreatment) to 2000 ppm NO for 15 min.

When NO TPD occurs in flowing O_2, the TPD spectrum shown in Fig. 6 shows no evidence of NO below 450 K and only an intense peak for N_2O. The infrared spectra in Fig. 3 show that over this temperature range, $H^+(NO_2^{\delta+})$ undergoes decomposition and peaks for nitrite and nitrate species grow monotonically. The absence of NO in the gas phase is presumably due to its very rapid conversion to either N_2O or NO_2. The latter of these two species is then rapidly adsorbed on the catalyst as nitrite and nitrate species. Above 450 K, NO appears in the gas phase. The infrared spectra show that the only source for this product is decomposition of $H^+(NO_2^{\delta+})$ species. Finally, above 600 K, there is a rise in the release of NO and the concurrent formation of a significant amount of NO_2. Consistent with the trends observed in the infrared spectra, the appearance of these products is attributed to the complete decomposition of the nitrite and nitrate species.

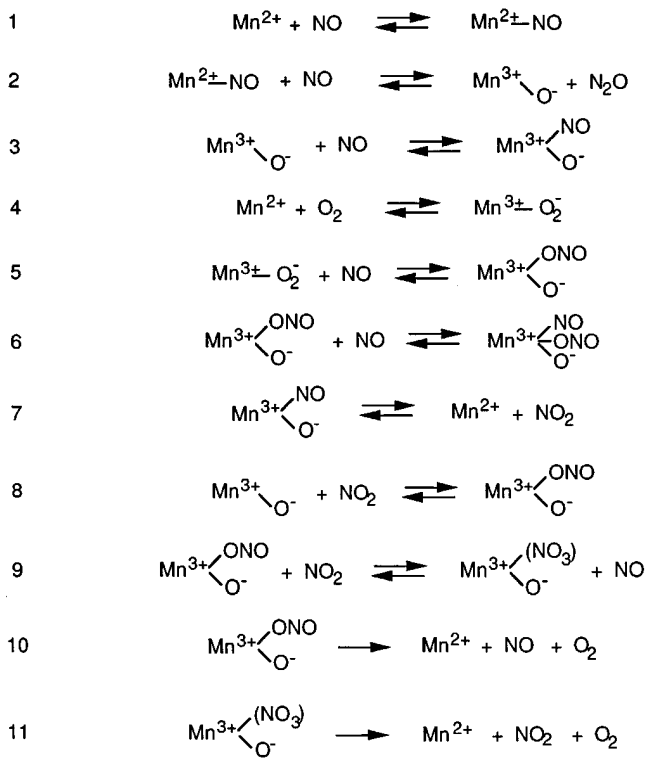

FIG. 7. Elementary processes proposed to explain the adsorption and desorption of NO.

Reduction of NO by CH_4

The activity measurements for NO reduction by methane over Mn-ZSM-5 are shown in Fig. 8. In the absence of

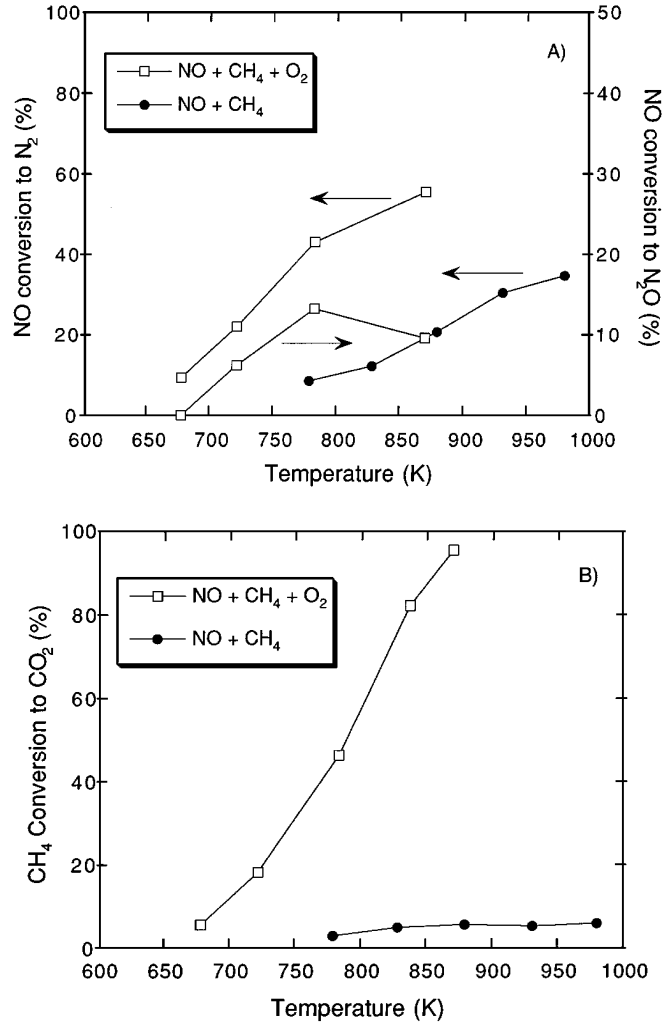

FIG. 8. NO (A) and CH_4 (B) conversion versus temperature. Feed composition: [NO] = 5000 ppm, [CH_4] = 5000 ppm, [O_2] = 2.0%. Total flow rate = 100 cm^3/min, GHSV = 15,000.

O_2 significant activity is observed above 773 K. The ratio of NO to CH_4 consumption increases from 2.8 to 5.8 as the temperature rises from 780 to 980 K. For comparison, this ratio should be 4.0 for the reaction $CH_4 + 4\,NO \rightarrow 2\,N_2 + CO_2 + 2\,H_2O$. When O_2 is present significant activity for NO reduction is seen above 673 K. At higher temperatures the CH_4 conversion to CO_2 increases more rapidly than the NO conversion to N_2, and the NO to CH_4 consumption ratio decreases from 1.7 to 0.58 as the temperature rises from 678 to 870 K. When O_2 is present, this ratio should be 2.0 for the reaction $CH_4 + 2\,NO + O_2 \rightarrow N_2 + CO_2 + 2\,H_2O$. Similar ratios of NO to CH_4 consumption have been reported previously for Co-ZSM-5 (2, 13, 21); the decline in this ratio with increasing temperature has been attributed to the production of CO_2 as a consequence of CH_4 combustion by O_2. However, in contrast to the behavior of Co-ZSM-5, and in agreement with results reported earlier (10), the curve of NO conversion versus temperature does not pass through a maximum. Mn-ZSM-5 exhibits a higher selectivity to N_2 than Co-ZSM-5 at temperatures above 773 K. N_2O formation is observed in the presence of O_2 only, with a lightoff temperature of 723 K, and maximum in conversion at 773 K.

To identify the species present on the catalyst surface under reaction conditions, infrared spectra were recorded as the temperature was raised from 298 to 773 K. Infrared spectra recorded during the passage of a mixture of NO and CH_4 over the catalyst are presented in Fig. 9. The room-temperature spectrum is similar to that shown in Fig. 1. As the temperature rises above 298 K the band for $Mn^{2+}(NO)$ disappears and the band for $Mn^{3+}(O^-)(NO)$ increases in intensity, passes through a maximum, and then attenuates. The bands for $H^+(NO_2^{\delta+})$ and nitrito species also grow in intensity and then pass through a maximum. Ramping the catalyst in NO alone leads to identical spectra up to 623 K, at which point the spectra become virtually featureless. But at 673 K, in the $NO + CH_4$ mixture, new bands appear at 2260, 2156, and 1630 cm^{-1}. The band at 1630 cm^{-1} is attributable to H_2O.

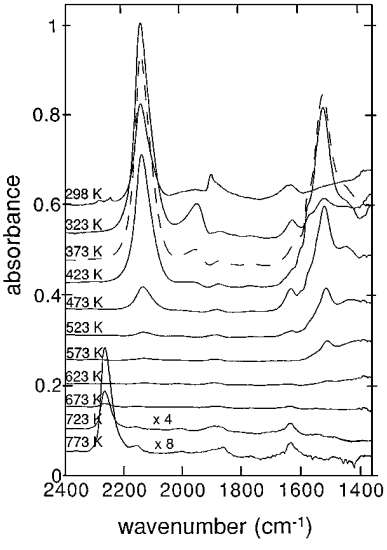

FIG. 9. Infrared spectra observed during the temperature-programmed reaction of a feed containing 5800 ppm NO and 9800 ppm CH_4 in He. The catalyst (standard pretreatment) is exposed to the reaction mixture for 20 min at room temperature prior to initiating the temperature ramp.

TABLE 1

Effect of Isotopic Composition of Feed Mixture on the Vibrational Frequencies of Adsorbed CN and NCO Species

Gas mixture	$\bar{\nu}_{NCO}$	$\bar{\nu}_{CN}$
$NO + CH_4$	2260	2156
$NO + {}^{13}CH_4$	2200	2114
$^{15}NO + CH_4$	2241	2123

The bands in Fig. 9 appearing at 2260 and 2156 cm^{-1} are similar to those observed over Co-ZSM-5 (22) when a mixture of NO and CH_4 is passed over the catalyst at temperatures above 623 K. Table 1 demonstrates that the positions of both bands shift when the feed mixture is switched from $^{14}NO + {}^{12}CH_4$ to $^{14}NO + {}^{13}CH_4$ or $^{15}NO + {}^{12}CH_4$ at 723 K. The redshift of the two bands when one of the reactants is isotopically labeled indicates that both features are due to species containing C and N atoms. The band at 2260 cm^{-1} is assigned to $Al^{3+}(NCO)$. Solymosi *et al.* have observed a similar band at 2260 cm^{-1} when Cu-ZSM-5 is exposed to HNCO (31) and Aylor *et al.* have attributed a band at 2270 cm^{-1} to $Al^{3+}(NCO)$ when Co-ZSM-5 is used to catalyze the reduction of NO by CH_4 (21). Assignment of the 2260 cm^{-1} band to NCO is consistent, as well, with the observation of a redshift to 2241 cm^{-1} when the species is ^{15}N labeled. The observed shift is in excellent agreement with the predicted shift of 2244 cm^{-1} assuming that NCO is treated as a pseudo-diatomic species (NC)–O. When the NCO group is ^{13}C labeled, the frequency shifts to 2200 cm^{-1}. This value is in fairly good agreement with the predicted value of the frequency, 2210 cm^{-1}, assuming a pseudo-diatomic of the form N(C–O). Based on our recent investigation of Co-ZSM-5 the band at 2156 cm^{-1} is attributed to CN species adsorbed on $Mn^{3+}(O^-)$ (22). This assignment is also consistent with the predicted shift to 2123 cm^{-1} for $^{12}C^{15}N$ and 2111 cm^{-1} for $^{13}C^{14}N$, in good agreement with the observed values of 2123 and 2114 cm^{-1}, respectively. The assignment of the band at 2156 cm^{-1} to $Mn^{3+}(O^-)(CN)$ is further supported by the stoichiometry of the products produced during transient reaction studies conducted with NO_2, O_2 and NO (*vide infra*).

Figure 10 shows a series of infrared spectra recorded as a function of temperature while a mixture containing NO,

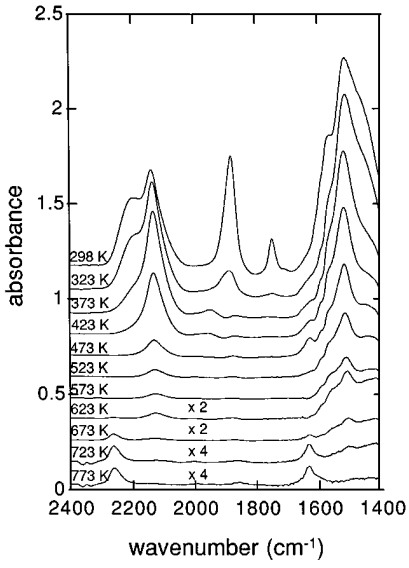

FIG. 10. Infrared spectra observed during the temperature-programmed reaction of a feed containing 5800 ppm NO, 1.1% O_2, and 1.0% CH_4 in He. The catalyst (standard pretreatment) is exposed to the reaction mixture for 20 min at room temperature prior to initiating the temperature ramp.

O_2, and CH_4 is passed over the catalyst. At room temperature new bands are present at 2189, 1877, and 1745 cm^{-1}, as well as a shoulder at 1558 cm^{-1}. The peak at 2189 cm^{-1} is most likely due to $NO_2^{\delta+}$ (32, 33), since this band is observed upon adsorption of NO_2 at room temperature. The bands at 1558 and 1877 cm^{-1} are due to N_2O_3 (34, 35), and that at 1745 cm^{-1} is indicative of N_2O_4 (36). All four of these new features disappear above 323 K. In contrast to what is shown in Fig. 9, when NO and CH_4 are passed over the catalyst there are very strong features observable for nitrito and nitrato species. This, along with the low stability of the band for adsorbed NO seen in Fig. 9, argues against NO disproportionation (see reactions 1–3, 7 in Fig. 7) as the source of adsorbed NO_2 in the steady-state reaction, and instead points toward the direct oxidation of NO (see reactions 4 and 5 in Fig. 7). As the temperature is raised to 623 K all of the infrared features disappear with the exception of the nitrito and nitrato bands, and above 673 K new bands appear at 2260 and 1630 cm^{-1} associated with $Al^{3+}(NCO)$ and H_2O, respectively. Spectra taken in a flow containing only NO and O_2 are identical to those shown in Fig. 10 up to 623 K. Above 623 K the intensity of the nitrito and nitrato bands are more intense in the absence of CH_4, and the bands at 2260 and 1630 cm^{-1} are not observed. These results suggest that the reaction of CH_4 with the nitrito and nitrato species leads to the attenuation in the intensity of the bands associated with these species and the appearance of the features for NCO, CN, and H_2O.

To test the hypothesis that the reduction of NO proceeds via the formation of NO_2 and the subsequent reduction of adsorbed NO_2 by CH_4, experiments were conducted in which NO_2 was first adsorbed at room temperature and the infrared cell then flushed with either He or CH_4 during the temperature ramp. Figures 11A and 11B show the results of these experiments. At 573 K, only NO_2 and NO_3 species are present on the catalyst in either case. Comparison of these spectra above 573 K, shows evidence of a reaction between $Mn^{3+}(O^-)(ONO)$ and CH_4, and the appearance of several new features. From 623 to 773 K, a new band appears at 2260 cm^{-1}. At 673 and 723 K there is also a band at 2156 cm^{-1} (see inset). As noted above, these new features are assigned to $Al^{3+}(NCO)$, and $Mn^{3+}(O^-)(CN)$, respectively. A small doublet centered at 2347 cm^{-1} due to CO_2 is seen at 723 K. The features at 1600 and 1576 cm^{-1} are in the range typical of C=O bonds (25) and are found to shift to 1550 and 1532 cm^{-1} when $^{13}CH_4$ is used. They can also be formed by ramping the temperature of the catalyst in a mixture of CH_4 and O_2. We tentatively assign these bands to carbonates (25). Their presence may indicate similarities between CH_4 combustion by O_2 and NO_2.

To ascertain whether $Al^{3+}(NCO)$ or $Mn^{3+}(O^-)(CN)$ might be intermediates in the reduction of NO by CH_4, a series of transient response experiments were performed. Isocyanate and cyanide bands were created in a mixture of 0.32% NO + 9.7% CH_4 at 723 K and then monitored while flowing 1% NO_2, NO, O_2, or pure He through the infrared cell. The decay of the adsorbed species was followed by infrared spectroscopy, and in a parallel experiment, production of reaction products was followed by mass spectrometry. Details have been given in an earlier publication (22).

Figure 12 shows the formation of N_2 and $^{13}CO_2$ as a function of time when the adsorbed species present on the catalyst surface are exposed to NO_2, NO, O_2, or pure He. In NO_2, the production of both $^{13}CO_2$ and N_2 occurs very rapidly, and any detectable production ceases after 50 s. In NO, N_2 is produced more rapidly than CO_2, but still much slower than is observed during the reaction in NO_2. Both $^{13}CO_2$ and N_2 are detectable as products for up to 10 min. In O_2, the production of $^{13}CO_2$ is more rapid than the production of N_2, but still much slower than in NO_2. However, the formation of both $^{13}CO_2$ and N_2 is faster in O_2 than in NO. The production of both $^{13}CO_2$ and N_2 is barely detectable in a flow of pure He. In all cases, N_2 and CO_2 were the primary reaction products, along with small amounts of N_2O.

Rate coefficients were determined by analysis of the rate of formation of $^{13}CO_2$ and N_2 (or the rate of decay of NCO and CN bands). In the case of the experiments carried out with O_2 and NO, the gas phase concentration of the reactant was virtually constant throughout the experiment, so that the apparent first order rate coefficient could be determined from the slope of a plot of the natural logarithm of product concentration (or IR band intensity) versus time. In the case where NO_2 is the reactant, correction must be made for the

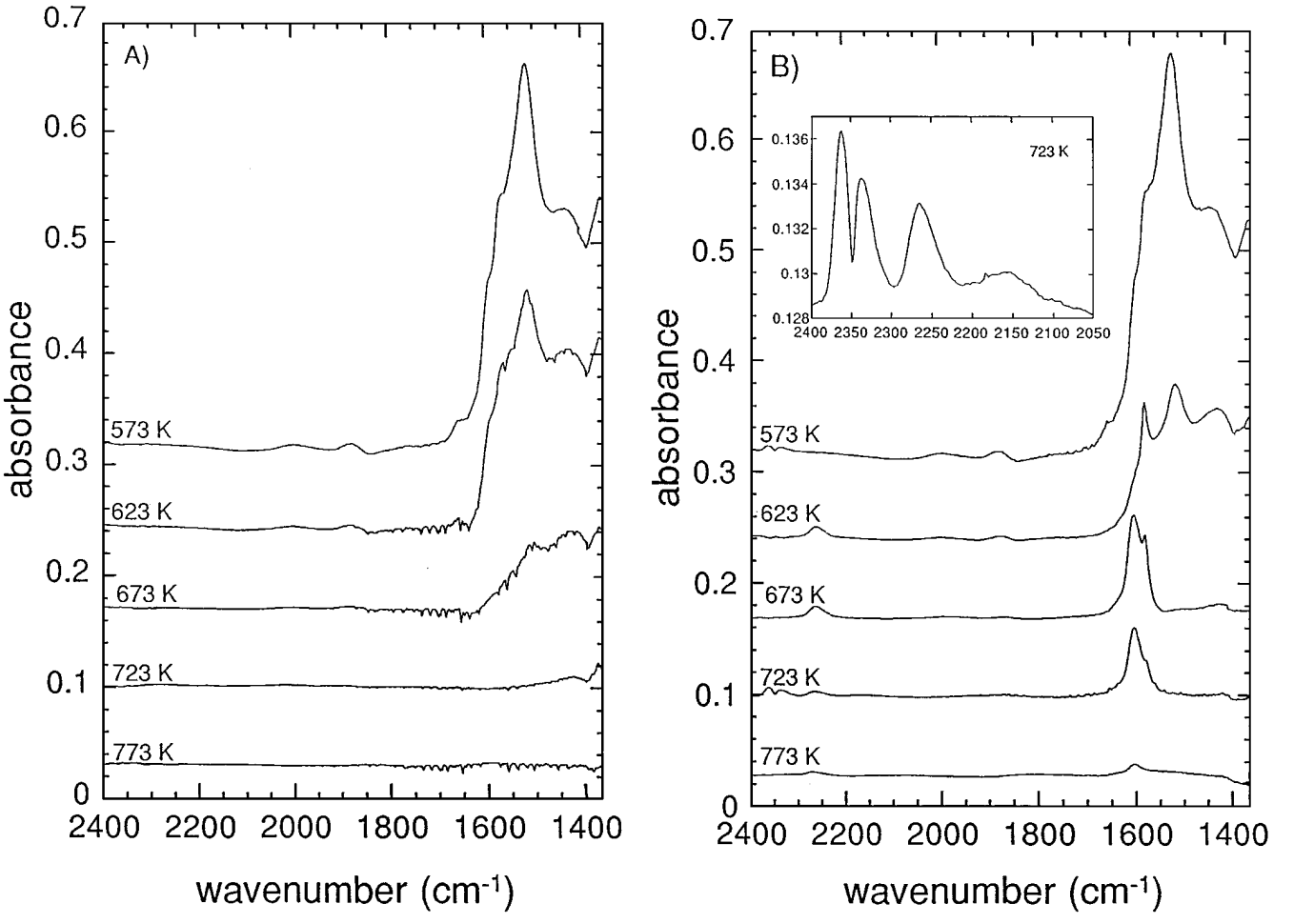

FIG. 11. Infrared spectra observed during the temperature-programmed desorption of NO_2 into He (A) and He containing 1.0% CH_4 (B), following room-temperature exposure of the catalyst (standard pretreatment) to 1.03% NO_2 for 20 min.

partial decomposition of NO_2 to NO and O_2, and for the consumption of gas phase NO_2. In all cases, the reaction of CN species was assumed to occur via an Eley–Rideal process. Values of the rate coefficients, k, determined by this means are listed in Table 2. When NO_2 is the reactant the magnitudes of the rate coefficients determined from the measurements of $^{13}CO_2$ and N_2 formation are very similar, suggesting that both products arise from a common precursor. Moreover, both rate coefficients are consistent in magnitude with that estimated from the decay in the intensity of the CN band, but much larger than the rate coefficient determined from the decay in the NCO band, leading to the conclusion that CN species are the primary source of N_2 and CO_2. In O_2, the rate coefficient for the consumption of CN agrees very well with the rate coefficient for CO_2 formation, once again pointing to CN as the precursor to CO_2. The rate coefficient for N_2 formation is smaller than that for CO_2 when O_2 is the reactant. This might reflect the fact that N_2 and CO_2 do not arise as the products of an elementary reaction in this case, but rather are produced via a sequence of steps. In NO, the rate coefficients for the consumption of both CN and NCO are about five times larger than the rate coefficients for the appearance of CO_2 and N_2. The reason for this discrepancy is unclear; however, it should be noted that the accuracy in determining the rate coefficient for the consumption of adsorbed species is not high in this case. As found previously for Co-ZSM-5 the rate coefficients for

TABLE 2

First Order Rate Coefficients for the Reaction of CN and NCO Species with NO, O_2, and NO_2

	Mass spectrometry (s^{-1} ppm^{-1})		Infrared spectroscopy (s^{-1} ppm^{-1})	
Purge gas	CO_2	N_2	NCO	CN
NO	8.1×10^{-8}	9.9×10^{-8}	4.4×10^{-7}	5.3×10^{-7}
O_2	1.1×10^{-6}	5.9×10^{-7}	1.5×10^{-7}	1.4×10^{-6}
NO_2	1.1×10^{-4}	1.2×10^{-4}	1.6×10^{-6}	$>10^{-5}$

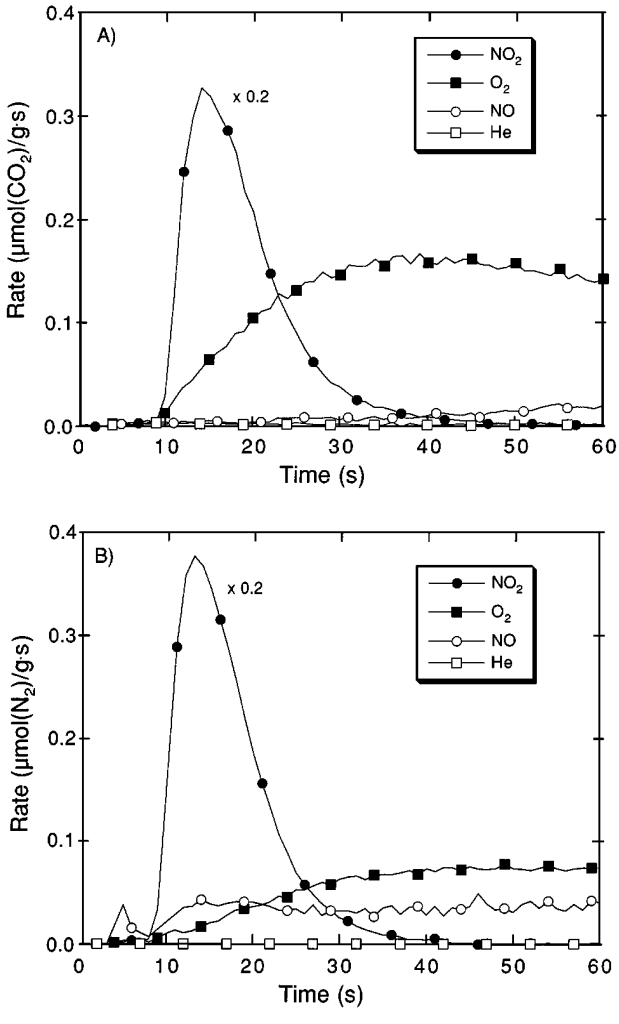

FIG. 12. Rate of $^{13}CO_2$ (A) and N_2 (B) formation as a function of time during the reaction of CN with NO_2, O_2, NO, and He.

the reaction of cyanide and isocyanide species in NO_2 are much greater than in NO or O_2, and the rate coefficient for the reaction of CN is at least an order of magnitude greater than that for NCO in either NO_2 or O_2.

The stoichiometry of the adsorbed species contributing to the formation of CO_2 and N_2 during the transient experiments can be determined from an analysis of the ratio of N_2 to $^{13}CO_2$ produced. As indicated in Table 3, the observed values of $N_2:{}^{13}CO_2$ are 1.11, 0.57, and 2.05, for reaction in NO_2, O_2, and NO, respectively. Also listed in Table 3 are the anticipated ratios of $N_2:CO_2$ assuming that CN or NCO species are the dominant source of CO_2 and N_2. The best agreement between the observed and the expected ratio is achieved when it is assumed that CN species are the dominant source of CO_2 and N_2. These results suggest that the extinction coefficient for the isocyanate group must be at least an order of magnitude greater than that for cyanide, consistent with what is found in the literature (37, 38), and

TABLE 3

Measured Ratio of N_2 to CO_2 for the Reaction of CN and NCO Species with NO, O_2, and NO_2

Purge gas	Amount desorbed (μmol) $^{13}CO_2$	Amount desorbed (μmol) N_2	Actual $N_2:{}^{13}CO_2$	Predicted $N_2:CO_2$ CN[a]	Predicted $N_2:CO_2$ NCO[b]
NO	1.08	2.21	2.05	1.5	1.0
O_2	1.91	1.08	0.57	0.5	0.5
NO_2	1.87	2.08	1.11	1.0	0.75

[a] Assuming the stoichiometry $CN + a(NO, O_2, \text{or } NO_2) \rightarrow bN_2 + cCO_2$.
[b] Assuming the stoichiometry $NCO + a(NO, O_2, \text{or } NO_2) \rightarrow bN_2 + cCO_2$.

in good agreement with what has been reported recently for Co-ZSM-5 (22).

Figure 13 illustrates a possible mechanism for the reduction of NO by CH_4 in the presence of O_2. The sequence begins with the adsorption of O_2 followed by NO to form a nitrito species (reactions 1 and 2). Adsorbed nitrito species are then available to react with methane forming adsorbed CH_3NO species with the release of hydroxyl radicals (reaction 3). Subsequent reaction of adsorbed nitrosomethane with OH radicals (reaction 4), followed by isomerization

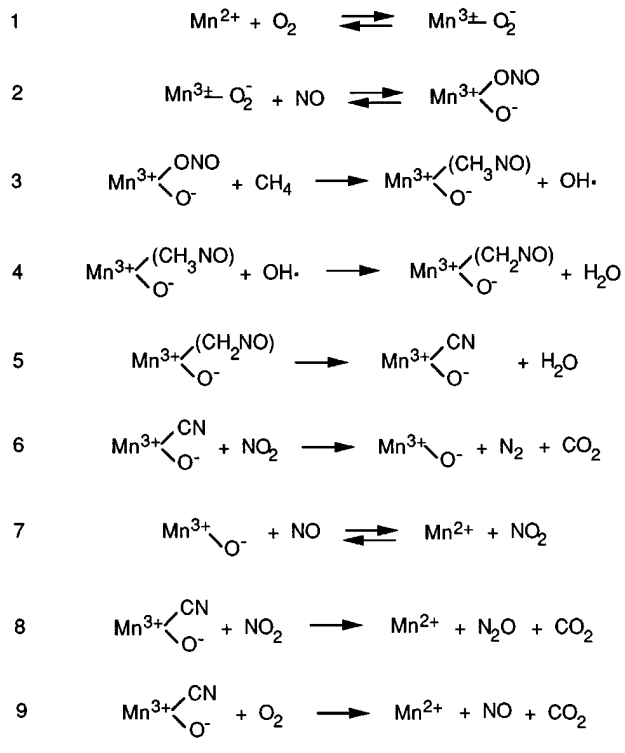

FIG. 13. Proposed reaction mechanism for NO reduction by CH_4 in excess O_2 over Mn-ZSM-5. Since the bonding of CH_3NO and CH_2NO to Mn is not known, these species are shown in parentheses.

and the elimination of water (reaction 5), is proposed as the path leading to the formation of adsorbed CN species. The cyanide species react with NO_2 to form N_2 and CO_2 (reaction 6) or to form N_2O and CO_2 (reaction 8). The reaction of cyanide species with O_2 (reaction 9) could result in the formation of NO and CO_2, contributing to the decline in selectivity observed at elevated temperatures.

The reaction sequence presented in Fig. 13 is similar to that proposed for Co-ZSM-5 (21). The principal differences are that Co does not undergo a change in oxidation state from 2+ and that N_2O is not observed over Co-ZSM-5. The possibility of adsorbed CH_3NO as an intermediate was suggested in the case of Co on the basis of previous studies (39) which showed that this species could be formed as a ligand by migratory insertion of NO into the Co–C or Ru–C bond of a CH_3 ligand. In related studies (40) it was demonstrated that upon heating, ligated CH_2NO decomposes to form CN and H_2O.

If CN species are the intermediates from which N_2 and CO_2 are formed, as suggested by reaction 6 in Fig. 13, then the rate of CN consumption via reaction in NO_2 should be equal to the overall rate of N_2 formation derived from the reduction of NO. Based on the published rate law of Li and Armor (10) the TOF for NO consumption at 773 K for the conditions of Fig. 10 is determined to be $9.0 \times 10^{-4}\ s^{-1}$. The surface coverage of cyanides expected under the conditions of Fig. 10 can then be determined from the relationship

$$\mathrm{TOF} = k_{NO_2}\theta_{CN}P_{NO_2}. \qquad [1]$$

Using K_{N_2} from Table 2 and assuming equilibrium conversion of NO and O_2 to NO_2 we determine $\theta_{CN} = 0.011$. The calculated value of θ_{CN} is below the detection limit of the infrared spectrometer and explains why CN species are not observed in Fig. 10. The calculation suggests, however, that the reactivity of CN with NO_2 is fast enough to consider CN as reaction intermediates.

CONCLUSIONS

The interaction of NO with Mn-ZSM-5, as well as the reduction of NO by methane, has been investigated using *in situ* infrared spectroscopy and temperature-programmed desorption and reaction methods. Adsorption of NO at room temperature on Mn^{2+} leads to the slow oxidation to Mn^{3+}, with the simultaneous formation of $Mn^{2+}(NO)$ and $Mn^{3+}(O^-)(NO)$ and the appearance of N_2O in the gas phase. Elevating the temperature or introducing O_2 converts the $Mn^{3+}(O^-)(NO)$ to NO_2/NO_3 species. Adsorbed NO_2/NO_3 species are more stable to high temperature than NO. During the reduction of NO by CH_4 in the presence of O_2, NO_2 is formed via the oxidation of NO. Adsorbed NO_2 then reacts with CH_4. Cyanide species are observed and found to react very rapidly with NO_2, leading to the formation of N_2 and CO_2. While isocyanate species are also observed, these species are associated with Al atoms in the zeolite lattice and do not act as reaction intermediates. A mechanism is proposed to account for the interaction of NO with Mn-ZSM-5 and for the reduction of NO by CH_4. As part of the reduction mechanism it is proposed that N_2 and CO_2 are formed via the reaction $Mn^{3+}(O^-)(CN) + NO_2 \rightarrow Mn^{3+}(O^-) + N_2 + CO_2$ and that N_2O and CO_2 are formed via the reaction $Mn^{3+}(O^-)(CN) + NO_2 \rightarrow Mn^{2+} + N_2O + CO_2$.

ACKNOWLEDGMENT

This work was supported (in part) by a grant from the Gas Research Institute under Contract 5093-260-2492. Facilities were provided by the Director of the Office of Basic Energy Sciences, Material Sciences Division, of the U.S. Department of Energy under Contract DE-AC03-76SF00098.

REFERENCES

1. Li, Y., and Armor, J. N., Catalytic Reduction of NO_x Using Methane in the Presence of Oxygen, U.S. Patent No. 5,149,512 (1992).
2. Li, Y., and Armor, J. N., *Appl. Catal. B* **1**, L31 (1992).
3. Nishizaka, Y., and Misono, M., *Chem. Lett.*, 1295 (1993).
4. Li, Y., Battavio, P. J., and Armor, J. N., *J. Catal.* **142**, 561 (1993).
5. Burch, R., and Scire, S., *Appl. Catal. B* **3**, 295 (1994).
6. Tabata, T., Kokitsu, M., and Osamu, O., *Catal. Lett.* **25**, 393 (1994).
7. Armor, J. N., and Farris, T. S., *Appl. Catal. B* **4**, L11 (1994).
8. Gopalakrishnan, R., Stafford, P. R., Davidson, J. E., Hecker, W. C., and Bartholomew, C. H., *Appl. Catal. B* **2**, 165 (1993).
9. d'Itri, J. L., and Sachtler, W. M. H., *Appl. Catal. B* **2**, L7 (1993).
10. Li, Y., and Armor, J. N., *Appl. Catal. B* **2**, 239 (1993).
11. Petunchi, J. O., and Hall, W. K., *Appl. Catal. B* **2**, L17 (1993).
12. Campa, M. C., DeRossi, S., Ferraris, G., and Indovina, V., *Appl. Catal. B* **8**, 315 (1996).
13. Witzell, F., Sill, G. A., and Hall, W. K., *J. Catal.* **149**, 229 (1994).
14. Li, Y., and Armor, J. N., *J. Catal.* **150**, 376 (1994).
15. Li, Y., Slager, T. L., and Armor, J. N., *J. Catal.* **150**, 388 (1994).
16. Kikuchi, E., and Yogo, K., *Catal. Today* **22**, 73 (1994).
17. Cowan, A. D., Dumpelmann, R., and Cant, N. W., *J. Catal.* **151**, 356 (1995).
18. Lukyanov, D. B., Still, G., d'Itri, J. L., and Hall, W. K., *J. Catal.* **153**, 265 (1995).
19. Li, Y., and Armor, J. N., *Appl. Catal. B* **5**, L257 (1995).
20. Adelman, B. J., Beutel, T., Lei, G.-D., and Sachtler, W. M. H., *J. Catal.* **158**, 327 (1996).
21. Aylor, A. W., Lobree, L. J., Reimer, J. A., and Bell, A. T., *in* "11th International Congress on Catalysis—40th Anniversary" (J. W. Hightower, W. N. Delgass, E., Iglesia, and A. T. Bell, Eds.), Studies in Surface Science and Catalysis, Vol. 101, p. 651. Elsevier, Amsterdam, 1996.
22. Lobree, L. J., Aylor, A. W., Reimer, J. A., and Bell, A. T., *J. Catal.*, in press.
23. Joly, J. F., Zanier-Szyldowski, N., Colin, S., Raatz, F., Saussey, J., and Lavalley, J. C., *Catal. Today* **9**, 31 (1991).
24. Aylor, A. W., Larsen, S. C., Reimer, J. A., and Bell, A. T., *J. Catal.* **157**, 592 (1995).
25. Nakamoto, K., "Infrared and Raman Spectra of Inorganic and Coordination Compounds," 4th ed., Wiley, New York, 1986.
26. Iwamoto, M., Yahiro, H., Mizuno, N., Zhang, W., Mine, Y., Furukawa, H., and Kagawa, S., *J. Phys. Chem.* **96**, 9360 (1992).
27. Valyon, J., and Hall, W. K., *J. Phys. Chem.* **97**, 7054 (1993).
28. Hoost, T. E., Laframboise, K. A., and Otto, K., *Catal. Lett.* **33**, 105 (1995).

29. Windhorst, K. A., and Lunsford, J. H., *J. Am. Chem. Soc. Faraday Trans. 1* **97**, 1407 (1975).
30. Lunsford, J. H., Hutta, P. J., Lin, M. J., and Windhorst, K. A., *Inorg. Chem*. **17**, 606 (1978).
31. Solymosi, F., and Bansagi, T., *J. Catal.* **156**, 75 (1995).
32. Evans, J. C., Rinn, H. W., Kuhn, S. J., and Olah, G. A., *Inorg. Chem*. **3**, 857 (1964).
33. Nebgen, J. W., McElroy, A. D., and Klodowsky, H. F., *Inorg. Chem*. **4**, 1796 (1965).
34. Chao, C.-C., and Lunsford, J. H., *J. Am. Chem. Soc.* **93**, 71 (1971).
35. Hisatsune, I. C., and Devlin, J. P., *Spectrochimica Acta* **16**, 401 (1960).
36. Begun, G. M., and Fletcher, W. H., *J. Molec. Spec.* **4**, 388 (1960).
37. Person, W. B., and Zerbi, G., "Vibrational Intensities in Infrared and Raman Spectroscopy," Vol. 20, Elsevier, Amsterdam, 1982.
38. Nakanishi, K., "Infrared Absorption Spectroscopy—Practical," Nankodo, Tokyo, 1962.
39. Weiner, W. P., and Bergman, R. G., *J. Am. Chem. Soc.* **105**, 3922 (1983).
40. Chang, J., Seidler, M. D., and Bergman, R. G., *J. Am. Chem. Soc.* **111**, 3258 (1989).